Inorganic Chemistry

pubs.acs.org/IC Article

Giant Magnetoelectric Coupling and Magnetic-Field-Induced Permanent Switching in a Spin Crossover Mn(III) Complex

Vibe B. Jakobsen, Shalinee Chikara, Jie-Xiang Yu, Emiel Dobbelaar, Conor T. Kelly, Xiaxin Ding, Franziska Weickert, Elzbieta Trzop, Eric Collet, Hai-Ping Cheng, Grace G. Morgan,* and Vivien S. Zapf*

Cite This: https://dx.doi.org/10.1021/acs.inorgchem.0c02789 Read Online

ACCESS | Metrics & More | Article Recommendations | Supporting Information

ABSTRACT: We investigate giant magnetoelectric coupling at a Mn^{3+} spin crossover in $[Mn^{III}L]BPh_4$ (L = $(3,5\text{-diBr-sal})_2323$) with a field-induced permanent switching of the structural, electric, and magnetic properties. An applied magnetic field induces a first-order phase transition from a high spin/low spin (HS-LS) ordered phase to a HS-only phase at 87.5 K that remains after the field is removed. We observe this unusual effect for DC magnetic fields as low as 8.7 T. The spin-state switching driven by the magnetic field in the bistable molecular material is accompanied by a change in electric polarization amplitude and direction due to a symmetry-breaking phase transition between polar space groups. The magnetoelectric coupling occurs due to a $\gamma\eta^2$ coupling between the order parameter γ related to the spin-state bistability and the symmetry-breaking order parameter η responsible for the change of symmetry between polar structural phases. We also observe conductivity occurring during the spin crossover and evaluate the possibility that it results from conducting phase boundaries. We perform ab initio calculations to understand the origin of the electric polarization change as well as the conductivity during the spin crossover. Thus, we demonstrate a giant magnetoelectric effect with a field-induced electric polarization change that is 1/10 of the record for any material.

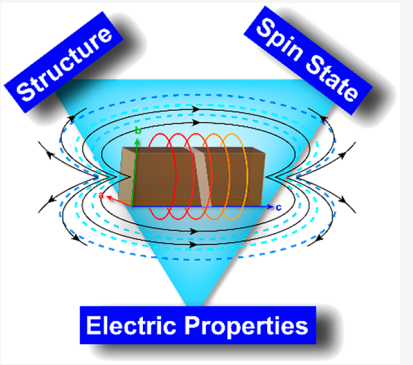

INTRODUCTION

Magnetoelectric (ME) coupling occurs when the magnetic field H influences the electric polarization P and dielectric constant and/or the electric field E influences the magnetization M. Applications include electric control of magnetic qubits as well as magnetic sensors, data storage, tunable antennas, and other frequency devices.[1−5] ME coupling is sought after in insulating materials since the large power dissipation from electric currents in conducting materials is eliminated.[2,6−8] To date, the necessary materials to satisfy all needed applications of ME coupling have not been found. Traditionally, it has been common to study ME coupling in inorganic oxides with ordered magnetic spin orientations, such as (anti)ferromagnets.[9,10] Here we demonstrate ME coupling in a molecule-based spin crossover (SCO) complex exhibiting magnetic-field-driven spin-state bistability.

In general, SCO occurs in transition-metal complexes with d^4−d^7 electrons, such as the S = 1 to S = 2 transition in Jahn−Teller active Mn^{3+}.[11−18] SCO is attractive for ME coupling since it can trigger large changes in lattice parameters due to the change in the orbital occupancy of d-shell ions. SCO complexes containing Mn^{3+} are particularly interesting due to the additional strain from Jahn−Teller effects in the HS state. SCO behavior is common mostly between ∼50 and 400 K in metal complexes with organic ligands since they can often accommodate the strain.[13,16,18−20]

Most metal−organic complexes that exhibit SCO are paramagnets; for example, there is no magnetic exchange that is significant compared to the energy scales of the SCO. However, spin crossover materials can show cooperative phase transitions since the spin states can couple to each other via strain.[16,21,22]

ME coupling in SCO materials is a relatively new field and has been reported in a few compounds including Mn(taa)[23−25] (H-induced ΔP), $[Fe(Htrz)_2(trz)](BF_4)$,[26] and $[Fe(H_2B(pz)_2)_2(bipy)]$[27] (E-induced ΔM). Another compound, $[Fe(bpp)_2]^{2+}$, shows ferroelectric and spin crossover behavior though coupling has not yet been demonstrated.[28] Magnetic-field-induced SCO has a longer history and has been studied in a number of materials. Most of these exhibit partial SCOs at very high magnetic fields (>30 T) achieved by pulsed magnets.[23,29−35] Recently, subnanometer SCO devices have been demonstrated with very fast switching speeds and no degradation after 10^7 cycles above room temperature, making these attractive for switching applications.[36,37] SCOs in hybrid

Received: September 18, 2020

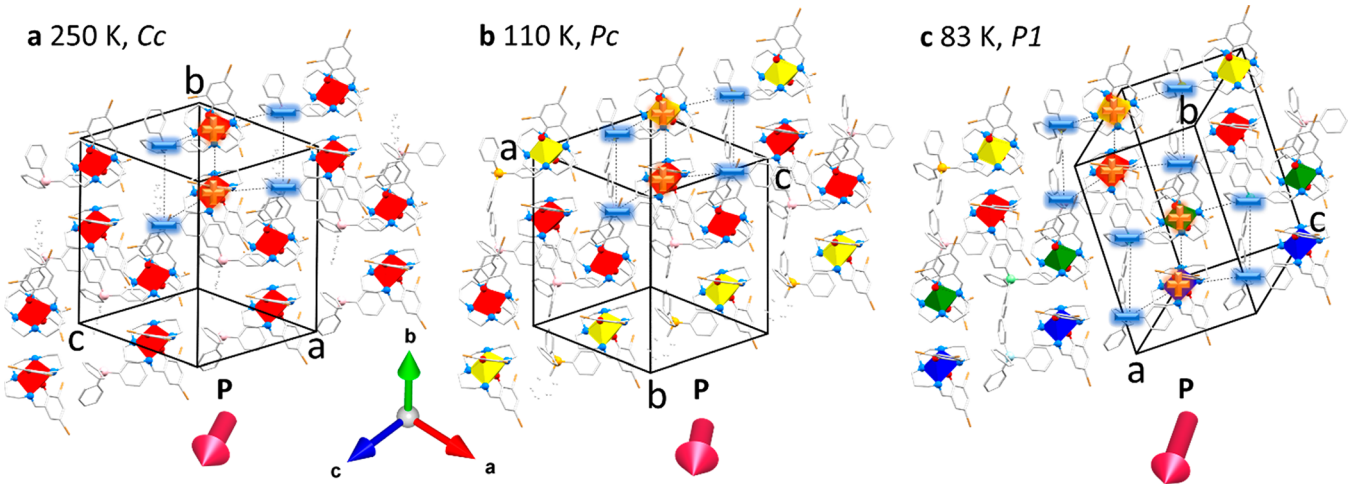

Figure 1. Packing diagrams of $[Mn^{III}L]BPh_4$ (**1**) with (a) HS *Cc* phase measured at 250 K, (b) HS *Pc* phase measured at 110 K, and (c) HS−LS *P*1 phase measured at 83 K. Mn^{3+} atoms are represented as polyhedra made up from six chelating donor atoms in (a−c), color-coded according to spin state as red (S = 2), yellow (S = 2), blue (S = 1), and green (S = 1). Structures are shown as stick figures. Donor atoms and the boron atom in the counteranion BPh_4^- are shown as ball-and-stick figures. Hydrogen atoms are omitted for clarity. The ionic centers are labeled (+, orange) and (−, blue). The thin dashed quadrilaterals show the distance between the cationic and anionic part of the molecule. The calculated direction and relative magnitude of bulk electric polarization P in the same reference frame (shown by the inset Cartesian coordinate axes) for all three phases are represented by the pink arrows below each subfigure and have a component along the *b*-axis only in the *P*1 phase. The packing diagrams with P in other orientations can be found in Figures S1−S3.

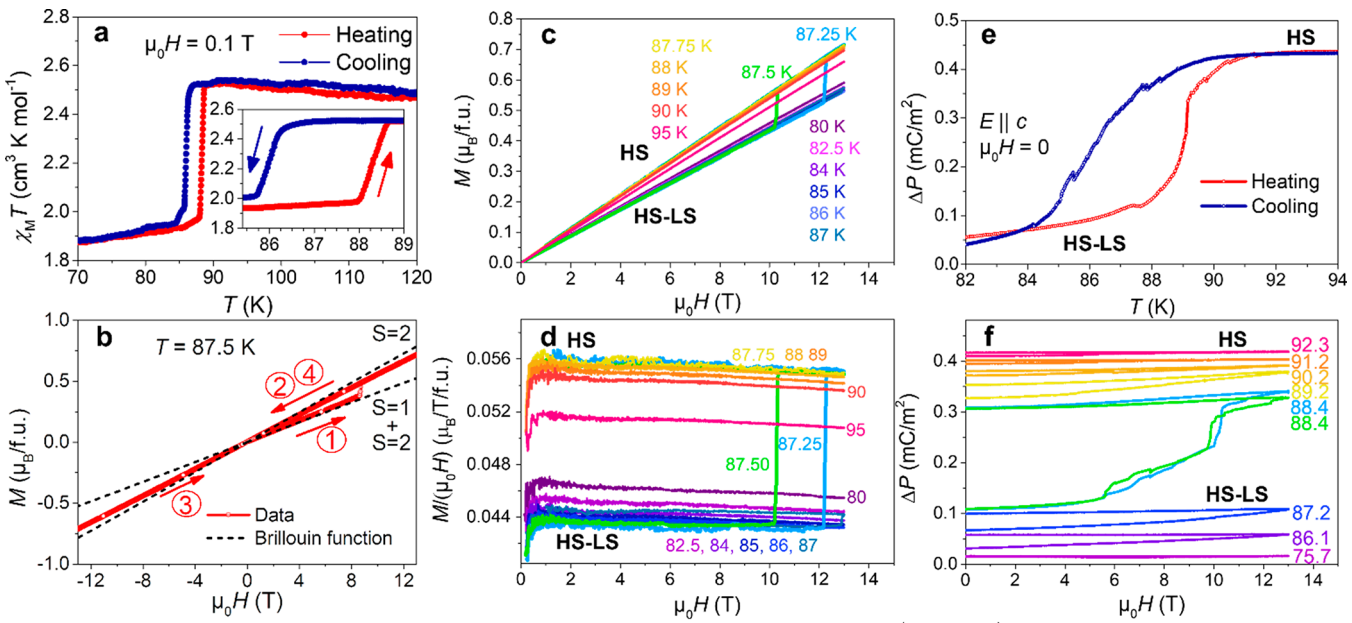

Figure 2. (a) $\chi_M T$ vs T of a single crystal for $H||c$ = 0.1 T with a zoomed-in view in the inset. (b) M vs $\mu_0 H$ (red points) showing a hysteretic H-induced SCO. Data were taken at T = 87.5 K with a history of warming from 70 K, measured for H swept from 0 to 13 T (1), 13 T to −13 T (2), −13 to 13 T (3), and 13 to 0 T (4) at 0.01 T s^{-1}. The Brillouin functions for HS S = 2 and for the HS−LS ordered state with a 1:1 ratio of the S = 1 and the S = 2 states are shown as dotted lines. The data show the SCO from the HS−LS ordered state to the HS state at 8.7 T on the first upsweep, and then the system remains in the HS state for the subsequent field sweeps. (c) $M(\mu_0 H)$ from 0 T−13 T−0 T at different temperatures T as indicated. $M(\mu_0 H)$ is measured with a history of warming from 70 K to the desired T as shown. (d) Same data plotted as $M/\mu_0 H$ for clarity. The H-induced SCO behavior can be seen at 87.5 and 87.25 K (thicker lines). (e) ΔP vs T at H = 0. (f) ΔP vs $\mu_0 H$ under the same experimental conditions of warming from 70 K. At 88.4 K, ΔP is shown twice to demonstrate the reproducibility of the switching. The jumps during the transition in ΔP are not noise; rather, they are observed in several different crystals and are likely due to polar domain reorientations. All data were measured with the long axis of the crystal, the *c*-axis in phase *Cc*, parallel to the field. Different samples were used in (a, b) and (c−f), resulting in different critical fields.

configurations with ferroelectrics or piezoelectrics are also a route to ME coupling, analogous to similar work in oxides.[38−40]

Here we report ME coupling at a cooperative SCO at a relatively low field of 8.7 T in the mononuclear Mn^{3+} complex $[Mn(3,5\text{-diBr-sal})_2323]BPh_4$ (abbreviated $[Mn^{III}L]BPh_4$ (**1**)).[41] The SCO is coupled to a structural phase transition between different polar space groups, resulting in a very large ME coupling. This material was previously reported to show an incomplete thermal SCO centered at 86 K between an S = 2/S

https://dx.doi.org/10.1021/acs.inorgchem.0c02789
Inorg. Chem. XXXX, XXX, XXX−XXX

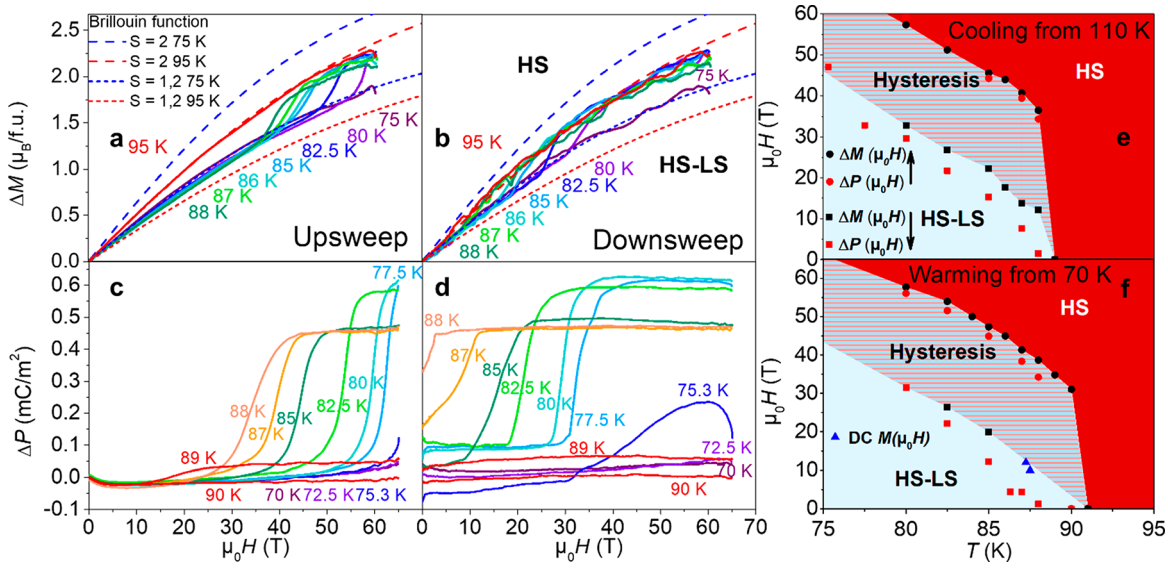

Figure 3. $M(H)$ in pulsed magnetic fields for (a) rising fields and (b) falling fields at different temperatures T as indicated after a history of cooling from 110 K. Dashed lines are Brillouin functions for the HS states (S = 2) with the upper blue and lower red lines for a given spin state corresponding to the lower and higher T, respectively. Similarly, short dashed lines show the Brillouin functions for the HS−LS ordered state. (c) $\Delta P(H)$ in a pulsed magnet for (c) rising fields and (d) falling fields. Data are measured after a history of cooling from 110 K to the final measurement T between every magnetic field pulse. Corresponding data with warming history are shown in Figures S9 and S10. (e) Pulsed field $H-T$ phase diagram showing the HS−LS ordered and HS states and the region of hysteresis in the first-order H-induced phase transition. Data are shown for a history of cooling from 110 K and warming from 70 K for (f). Data points in the phase diagram are determined from the midpoint in the H of the transition for pulsed field polarization (red dots) and magnetization curves (black dots), respectively. Arrows in the legend indicate whether H is sweeping up or down. Oscillations in the downsweep data are due to mechanical vibrations.

= 1 state (HS−LS) and a higher temperature (>90 K) pure S = 2 (HS) state of Mn^{3+}. The low-temperature phase is a polar $P1$ phase with a structurally ordered 1:1 ratio of LS and HS Mn^{3+} sites, while the higher temperature phase in space group Pc contains two HS Mn^{3+} sites (Figure 1a−c). An additional Cc HS phase forms above 250 K. We present electric polarization and magnetization experiments on single crystals in DC fields up to 13 T as well as millisecond pulsed fields up to 65 T along with ab initio calculations of the magnitude and directions of the electric polarization vector (Figure 1a−c).

RESULTS AND DISCUSSION

Magnetization and Electric Polarization. The magnetic susceptibility of a single crystal of **1**, plotted as $\chi_M T$ vs T, manifests a SCO as a sharp increase in $\chi_M T$ centered at 88 K on warming ($T_{1/2}\uparrow$ = 88 K) and at 86 K on cooling ($T_{1/2}\downarrow$ = 86 K). Values of $\chi_M T$ are consistent with the HS−LS and HS spin states (Figure 2a).[41] $M(H)$ was measured at T = 87.5 K in DC fields while H was swept from 0 → 13 → −13 → 13 → 0 T. The Brillouin functions in the HS−LS and HS states are shown as dotted lines. The slight deviation from the data is consistent with demagnetization factors in this irregular crystal with sharp corners. These data show that after an applied magnetic field switches the system to the HS state, the sample remains in this HS state even if the magnetic field is removed as long as temperature remains unchanged (Figure 2b).

H-induced SCO behavior has most often been reported above 30 T, achieved with capacitor-driven pulsed magnets.[25,29,34,42] Thus, the observation of SCO behavior as low as 8.7 T is unusual.[23] Moreover, the hysteretic "trapping" of the HS state is also a significant finding. Such trapping is usually only observed when these materials are exposed to light (light-induced excited spin-state trapping (LIESST)).[43−45] In the case of complex **1**, the spin state is switched with a magnetic field in a permanent hysteretic fashion. This permanent switching can occur in two scenarios: (1) the system is initially in the ordered spin (HS−LS) state in zero field at 87.5 K, but that state is a metastable excited state of the free energy at zero field. The magnetic field then assists the transition toward the HS stable state, which remains permanent after the field is removed. Alternatively, in scenario (2) the HS−LS ground state initially present at zero field transitions to a new HS ground state in applied H. After removal of H, the system remains trapped in the now metastable excited HS state. The latter case could be termed magnetic-field-induced spin-state trapping (MIESST).

One example was shown in a figure by Nakano et al.[23] but was not investigated further. Such switching should, however, be a general feature inside the region of bistability of the temperature hysteresis.

We further investigate the H-induced switching at different T in Figure 2c,d. The data were taken with a history of warming from 70 K to the measurement T, while data with a cooling history from 110 K are shown in Figure S6. The data demonstrate that the switching occurs for T = 87.25 and 87.5 K, in the immediate vicinity of T_c.

We have considered and eliminated several potential artifacts that could contribute to the permanent switching: T was kept stable during the measurement; the data are independent of the H sweep rate for dH/dt = 2, 5, and 10 mT s^{-1} (see Figures S7 and S8); and the possibility of substrate strain contributing to the hysteresis was eliminated by also measuring loose crystals, as described in the Supporting Information.

The ME coupling is investigated in Figure 2e,f, showing the electric polarization change ΔP along the c-axis that accompanies the SCO as a function of T and H, respectively. Similar to M, ΔP shows trapping of the HS state after removal

https://dx.doi.org/10.1021/acs.inorgchem.0c02789
Inorg. Chem. XXXX, XXX, XXX−XXX

of H. The steps and breadth of the transition in P were reproduced in several samples—they may result from polar domain reorientations. Indeed, in the Pc HS phase, P lies in the ac-plane, while in the $P1$ phase two ferroelastic domains form with an additional component of P along $\pm b$ due to the loss of the glide plane.

Notably $\Delta P(H)$ in **1** is giant—of the same order of magnitude as in Mn(taa),[25] significantly larger than that of most molecule-based magnetic materials,[46−51] and about 1/10 of the record for any material.[52] Additional electric polarization and dielectric constant data are shown in the Supporting Information along with an extended discussion of how artifacts are ruled out.

Magnetic and electric properties in high fields using capacitor-driven pulsed magnets were also measured to explore the phase diagram over a broader T and H range. Figure 3 shows $\Delta M(H)$ and $\Delta P(H)$ up to 65 T. In Figure 3a,b, $\Delta M(H)$ is shown for upsweeps and downsweeps of H together with the Brillouin functions expected in the HS−LS ordered and HS states. Here the high field can induce SCO also outside the thermal region of bistability, down to 75 K in $\mu_0 H$ up to 65 T. $\Delta P(H)$ in pulsed fields is shown for up- and downsweeps of the field (Figure 3c,d). $\Delta M(H)$ and $\Delta P(H)$ show transitions consistent with each other.

In agreement with the DC field data, we observe an apparent permanent switching effect in the data with a history of warming. However, in evaluating H-induced switching effects, we note that whereas we can be certain of T stability in DC measurements by comparing data taken with different long temperature stabilization times, we cannot guarantee T stability in pulsed fields since there is limited time to thermalize the sample. The SCO can generate heating or cooling due to entropy changes or irreversible heating effects. Thus, we report H-induced switching in DC fields but do not confirm it in pulsed fields.

Phase Diagram. The phase transitions in DC and pulsed fields are summarized in the $H-T$ phase diagram in Figure 3e,f. The H-induced SCO and its accompanying ME effects can be observed for two T regimes: (1) within the region of bistability and (2) outside it. Within the bistable region, the slope of the $H-T$ phase boundary is steepest. Because it is a first-order phase transition, the two phases have similar energies separated by an energy barrier. A change in H or T then alters the free energy landscape until it becomes energetically favorable for the new phase to overcome the barrier, nucleate, and propagate.

The second T regime occurs outside the region of bistability, well below $T_{1/2}$. Here, the slope of the $H-T$ phase boundary abruptly becomes much shallower. In this T regime, there is a free energy difference between the HS/LS and the HS state that must be closed by the Zeeman effect, which determines the slope of the phase diagram. Once the magnetic field closes the free energy gap, the mechanism described in the previous paragraph takes over. These two mechanisms can be expected to create different slopes in the $H-T$ phase diagram. From a mean-field extrapolation we estimate that H needed to induce the SCO at zero T in pulsed fields is ∼150 T. Finally, we note that in the compound Mn(taa) and other SCO materials with first-order phase transitions, the transitions in pulsed magnets are pushed to higher fields than in DC magnets because of the competition between the speed of the pulse and the speed of domain nucleation and growth.[25,53−60]

One particularity of the present system is that we observe ME coupling in a system with two coupled order parameters: (1) the high spin fraction γ and (2) the symmetry-breaking structural order parameter η that describes the HS−LS order and which is associated here with a ferroelastic shear as the HS−LS order implies the loss of the c glide plane. In the HS phase, $\gamma = 1$ and $\eta = 0$, while in the HS−LS phase the symmetry-allowed $\gamma\eta^2$ coupling term stabilizes $\gamma = 1/2$ and $\eta \neq 0$.[41,61,62] It is the coupling between the spin state and the structure that causes the SCO to become a first-order phase transition, as opposed to a gradual crossover. In the present case, η allows for ΔP along a, b, and c. As H drives switching from $\gamma = 1/2$ to $\gamma = 1$, $\gamma\eta^2$ also tunes a symmetry change between the HS−LS ordered phase and the HS phase and consequently the orientation of P.

Calculations of the Electric Polarization. The origin of the measured ΔP along the c-axis is a structural phase transition between polar space groups during which molecules tilt and distort, with the Jahn−Teller distortion being a dominant contribution.[41] Because of symmetry rules, the polarization vector must be in the a,c-plane of the HS Cc and Pc structures. As the c glide plane is lost in the HS−LS $P1$ structure, the lattice vector b is no longer perpendicular to a and c, which allows the polarization along b to become nonzero and of opposite sign between the ferroelastic domains.

We have calculated ΔP by a density functional approach based on the changes in crystal structures and spin states of **1** (Table 1). We perform these calculations for the three phases:

Table 1. Calculated ΔP of 1 in the Coordinate System of the HS Cc Phase for All Three Structural Phases[a]

phase	HS−LS	HS	HS
temperature	4−83 K	83−250 K	>250 K
lattice	triclinic	monoclinic	monoclinic
space group	$P1$ (1)	Pc (7)	Cc (9)
P_a (e Å uc^{-1})	4.78	3.72	2.74
P_b (e Å uc^{-1})	0.29	0.00	0.00
P_c (e Å uc^{-1})	8.75	5.50	6.74
P_a (mC m^{-2})	18.0	13.9	10.0
P_b (mC m^{-2})	1.10	0.00	0.00
P_c (mC m^{-2})	33.0	20.6	24.7

[a]The values are given along the principal axes of the HT phase.

$P1$ (HS−LS) below 83 K, Pc (HS) between 83 and 250 K, and Cc (HS) above 250 K.[41] To compare ΔP, the calculations were all performed in the unit cell orientation of the HS Cc phase.

The component of P along the b-axis (relative to the HS Cc phase) is zero for both HS Cc and Pc phases while it has a nonzero value of 1.1 mC m^{-2} for the HS−LS ordered $P1$ phase. The calculated value is an order of magnitude larger than the measured value. Such discrepancies are commonly seen in ferroelectric materials and may result from domain formation in the real crystal. In the present case we directly observed the formation of ferroelastic domains with opposite polarization components along the b-axis in X-ray diffraction experiments.[41] Thus, if domain-free crystals could be created, even larger ME effects would be expected.

Conductivity during the SCO. We have investigated the effects of applied electric fields E on the electric polarization. At a constant T and $H = 0$, measurements of $P(E)$ did not show any ferroelectric hysteresis for E up to 200 kV m^{-1}. This is very likely due to the fact that switching of the electric

https://dx.doi.org/10.1021/acs.inorgchem.0c02789
Inorg. Chem. XXXX, XXX, XXX−XXX

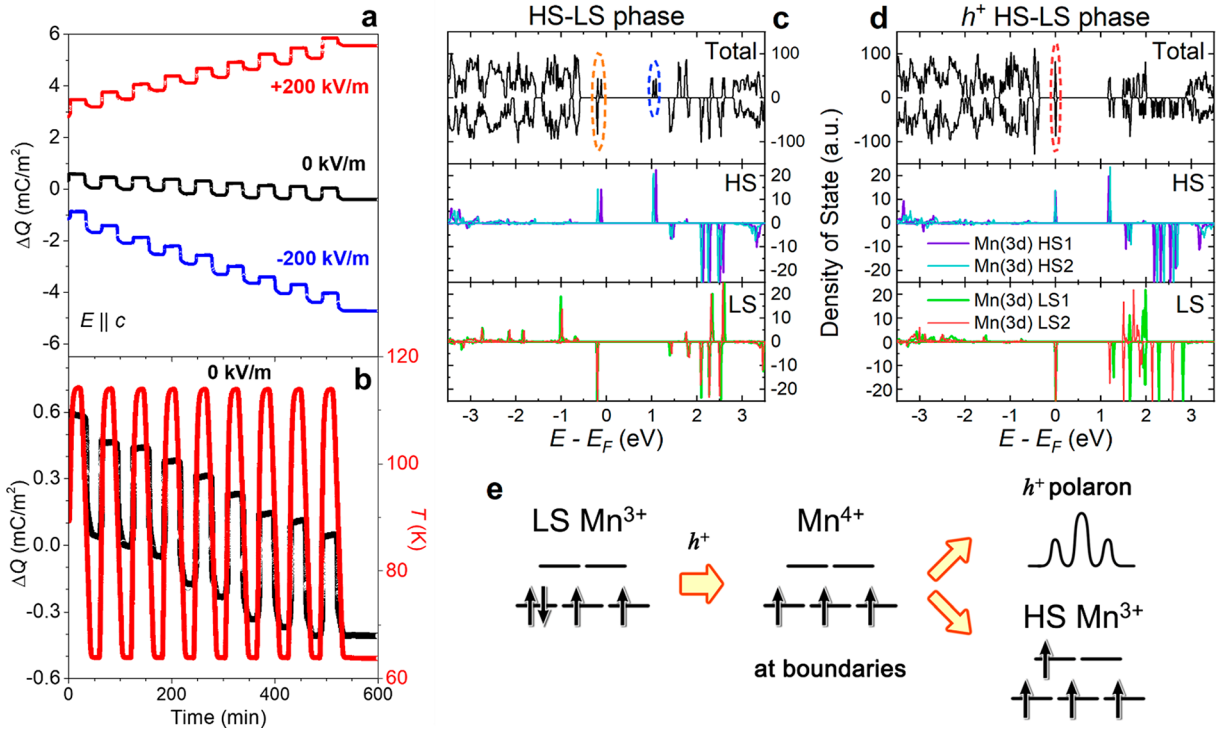

Figure 4. Evidence of conductivity during SCO (**1**). (a) Change in surface charge ΔQ as the temperature T is swept up and down between 65 and 100 K across the SCO temperature $T_{1/2}$, measured while applying electric fields E of 0, 200, and −200 kV m^{-1}. (b) T vs time on the right axis and ΔQ for $E = 0$ on the left axis corresponding to the data in (a). We interpret ΔQ as containing two components: a change in electric polarization ΔP occurring at the SCO phase transition that is of similar size for increasing and decreasing T and a voltage induced current that occurs at the moment of the phase transition. Standard errors are smaller than line widths. (c) (upper) the total DOS and projected DOS (PDOS) for (middle) HS and (lower) LS Mn(3d) in the HS−LS ordered phase. Positive and negative values refer to the spin-majority and spin-minority channel, respectively. The dashed orange and blue circles refer to HOMO and LUMO, respectively. In each case, zero energy is defined to be the Fermi energy, and is located at the top of HOMO. (d) Same as (c) but for the h$^+$-doped HS−LS ordered phase. Here, the dashed red circles indicates the Fermi level. (e) Schematic of how extra charge at the phase boundary can create a polaron.

polarization is associated with switching of ferroelastic domains. However, we do find conductivity occurring during the SCO. Figure 4a,b shows the change in charge ΔQ measured while crossing the SCO as a function of T. The quantity ΔQ is the total charge that flows to the sample's capacitor plates during a measurement and is usually equal to the electric polarization change ΔP. However, here we refer to this data as ΔQ rather than ΔP because we suspect there is an additional contribution to the total charge from current passing *through* the sample due to conductivity during the SCO. Figure 4a,b shows $\Delta Q(t)$ in a constant E of 0, 200, or −200 kV m^{-1}, measured while T was swept up and down across $T_{1/2}$. The $\Delta Q(t)$ plot reflects the expected ΔP when crossing the SCO, plus an additional component occurring only at the SCO. This second component follows the sign of E and is irreversible, causing ΔQ at the SCO to climb with each successive T sweep. Because it is unlikely that ΔP increases continuously to infinity, it is more likely that the sample becomes conducting during the process of the phase transition allowing charge to pass through the sample. We estimate that the resistivity of the millimeter-sized sample must drop to a few GΩ (hundreds of MΩ·cm) during the SCO for this effect to occur. *On the other hand, the samples are robustly insulating with resistances greater than TΩ and loss tangents of <1 × 10^{-5}outside the region of the SCO*. We were unable to capture the conducting phase by pausing the temperature sweep.

Thus, a likely source of the conductivity is the dynamic phase boundary that forms between the HS−LS ordered phase and the HS phase during the reconstructive first-order phase transition. This phase boundary is ferroelastic, and such phase boundaries between polar phases can often be charged and/or conducting.[41,63−65]

We performed density of states (DOS) calculations to investigate the effect of extra charges at the phase boundary. The extra charge can oxidize or reduce Mn^{3+} to Mn^{4+} or Mn^{2+}, respectively, depending on the sign of the charge. We focused our calculations on the Mn^{3+} ions that transition from LS to HS during the SCO. Figure 4c,d shows the DOS and the projected density of state (PDOS) of Mn(3d) orbitals in the HS−LS ordered phase and in the HS phase. If the phase boundary is negatively charged, the added electron can only be located at the lowest unoccupied molecular orbital (LUMO). This is the spin-majority Mn(3d) orbital of the HS state (the blue circle), whose spin state is unchanged during the phase transition, making negatively-charged boundaries trivial. If the boundary is positively charged, the added hole or positive charge can be located at the highest occupied molecular orbital (HOMO), which is the spin-majority Mn(3d) orbital set of the HS or the spin-minority Mn(3d) of the LS (the orange circle).

Figure 4d shows the DOS results of the HS−LS ordered phase with one h$^+$ per unit cell doped. The total magnetization is 12.5 μ_B; namely, about 0.75 h$^+$ are doped on spin-minority LS Mn^{3+}, and 0.25 h$^+$ are doped on spin-majority HS Mn^{3+}, so that the LS Mn^{3+} has high probability of being activated into Mn^{4+} with positively-charged boundaries. Furthermore, with the doped charge, the HOMO with double degeneracy (the

https://dx.doi.org/10.1021/acs.inorgchem.0c02789
Inorg. Chem. XXXX, XXX, XXX−XXX

red circle) at each spin channel lies at the Fermi level because there are two LS and two HS Mn^{3+} in one unit cell. This does not necessarily mean that a metallic band structure emerges at the charged boundaries.[66,67] Rather, given the GΩ resistance and molecular nature of the crystal, we postulate conduction by polaron hopping, which is the quasi-particle carrier in many conductive molecules[68,69] including SCO materials.[70,71] After the optimization of the h^+-doped structure, the splitting of those peaks is only 5 meV for spin majority and 10 meV for spin minority, respectively. This difference between two LS or two HS Mn(3d) orbitals at the Fermi level is tiny. It indicates that one unit cell cannot trap one hole at the measured temperatures, and thus it is more likely that polarons are dynamic with large sizes. During the SCO, the energy released by the change in phonon spectrum and from the formation of boundaries is large enough to generate polarons. Once a positive polaron is formed, the activated Mn^{4+} transforms to HS Mn^{3+}. Figure 4e displays how a LS Mn^{3+} at the positively charged boundaries becomes HS Mn^{3+} and meanwhile generates one positive polaron in the framework of our theory. The diffusion of polarons can further activate nearby LS Mn^{3+}, so that it accelerates the SCO with lower energy. To confirm this, we excite one of two LS Mn^{3+} into the HS with one h^+ doping. The total energy increases by merely 8 meV. This energy difference is smaller than that of the undoped situation (22 meV) and is also smaller than the SCO energy per Mn between the HS−LS ordered and HS phase (31 meV). It indicates that the charged boundaries can reduce the energy required for the SCO.

CONCLUSION

In conclusion, we have demonstrated cross-coupling between spin state, structure, and electric polarization in the Jahn Teller complex $[Mn^{III}L]BPh_4$(**1**). Near the SCO critical temperature, we observe magnetic-field-induced permanent switching of the spin state, structure, and electric polarization due to a first-order phase transition. The SCO behavior, monitored through the evolution of the HS fraction γ from 1/2 to 1, is driven by a field as low as 8.7 T, which is remarkably low compared to most other magnetic-field-induced SCO materials. Because of the $\gamma\eta^2$ coupling, the HS state stabilizes the high-symmetry phase with $\eta = 0$ and consequently suppresses the polarization component along the *b*-axis. We also note that conductivity is observed during the SCO, though not outside of it, and likely originates from polaron hopping at the charged phase boundaries forming during the first-order reconstructive phase transition that accompanies the SCO. $\Delta P(H)$ is 1/10 of the record for any material.[52] Thus, the combination of relatively low magnetic field switching and giant ME coupling showcases the potential for multifunctionality and applications in SCO materials.

ASSOCIATED CONTENT

Supporting Information

The Supporting Information is available free of charge at https://pubs.acs.org/doi/10.1021/acs.inorgchem.0c02789.

Methods for experimental measurements and discussion of artifacts, additional crystal structure depictions, additional data on magnetization, dielectric constant and electric polarization, and details of the density of states calculations (PDF)

AUTHOR INFORMATION

Corresponding Authors

Vivien S. Zapf − *National High Magnetic Field Lab, Los Alamos National Laboratory, Los Alamos, New Mexico 87545, United States;* orcid.org/0000-0002-8375-4515; Email: vzapf@lanl.gov

Grace G. Morgan − *School of Chemistry, University College Dublin, Dublin, Ireland;* orcid.org/0000-0002-5467-0507; Email: grace.morgan@ucd.ie

Authors

Vibe B. Jakobsen − *School of Chemistry, University College Dublin, Dublin, Ireland;* orcid.org/0000-0003-0671-092X

Shalinee Chikara − *National High Magnetic Field Lab, Los Alamos National Laboratory, Los Alamos, New Mexico 87545, United States*

Jie-Xiang Yu − *Department of Physics, University of Florida, Gainesville, Florida 32611, United States;* orcid.org/0000-0002-3739-3253

Emiel Dobbelaar − *School of Chemistry, University College Dublin, Dublin, Ireland;* orcid.org/0000-0002-5650-9231

Conor T. Kelly − *School of Chemistry, University College Dublin, Dublin, Ireland;* orcid.org/0000-0003-0465-2412

Xiaxin Ding − *National High Magnetic Field Lab, Los Alamos National Laboratory, Los Alamos, New Mexico 87545, United States*

Franziska Weickert − *National High Magnetic Field Lab, Los Alamos National Laboratory, Los Alamos, New Mexico 87545, United States*

Elzbieta Trzop − *CNRS, IPR (Institut de Physique de Rennes), UMR 6251, Univ. Rennes, F-35000 Rennes, France*

Eric Collet − *CNRS, IPR (Institut de Physique de Rennes), UMR 6251, Univ. Rennes, F-35000 Rennes, France;* orcid.org/0000-0003-0810-7411

Hai-Ping Cheng − *Department of Physics, University of Florida, Gainesville, Florida 32611, United States*

Complete contact information is available at: https://pubs.acs.org/10.1021/acs.inorgchem.0c02789

Author Contributions

V.S.Z. led the project. V.S.Z., S.C., and G.G.M. conceived the project. V.B.J. grew the crystals, performed the characterization, and analyzed the majority of the data in consultation with V.S.Z., J.Y. and H.C. performed calculations. V.S.Z. and S.C. designed the magnetoelectric experiments. S.C., E.D., C.K., and X.D. also performed data collection and analysis. F.W. built and provided a magnetization probe for some of the measurements. E.T. and E.C. collected and analyzed the single crystal X-ray diffraction data. V.B.J. and V.S.Z. wrote the manuscript with help from S.C., J.Y., H.C., and E.C. All authors have given approval to the final version of the manuscript.

Funding

The scientific work by V.S.Z., H.P.C., and J.Y. was funded by the Center for Molecular Magnetic Quantum Materials (M2QM), an Energy Frontier Research Center funded by the U.S. Department of Energy, Office of Science, Basic Energy Sciences under Award DE SC0019330. G.G.M. thanks Science Foundation Ireland (SFI) for support via an Investigator Project Award (19/FFP/6090). V.B.J. was supported by the

Irish Research Council GOIPG/2016/73 fellowship. Travel grants for V.B.J.'s research visits to LANL and IPR were funded by Augustinus Fonden (Grant No. 18-0338), Oticon Fonden (Grant No. 17-3813), Reinholdt W. Jorck og Hustrus Fond (Grant No. 18-JI-0573), P.A. Fiskers Fond, A.P. Møller og Hustru Chastine Mc-Kinney Møllers Fond til almene Formaal, and Christian og Ottilia Brorsons Rejselegat for yngre videnskabsmænd og-kvinder. C.T.K. was supported by the Irish Research Council GOIPG/2018/2510 and UCD Advance PhD Scheme Supplemental Award. The NHMFL experimental facility at LANL is funded by the U.S. National Science Foundation through Cooperative Grant DMR-1157490, the State of Florida, and the U.S. Department of Energy.

Notes

The authors declare no competing financial interest.

■ ACKNOWLEDGMENTS

The authors acknowledge Michael A. Carpenter, University of Cambridge, and Jia Chen, University of Florida, for helpful scientific discussions.

■ REFERENCES

(1) Wang, Y.; Li, J.; Viehland, D. Magnetoelectrics for magnetic sensor applications: status, challenges and perspectives. *Mater. Today* **2014**, *17* (6), 269−275.
(2) Heron, J. T.; Schlom, D. G.; Ramesh, R. Electric field control of magnetism using BiFeO3-based heterostructures. *Appl. Phys. Rev.* **2014**, *1* (2), 021303.
(3) Carman, G. P.; Sun, N. Strain-mediated magnetoelectrics: Turning science fiction into reality. *MRS Bull.* **2018**, *43* (11), 822−828.
(4) Pan, C.; Naeemi, A. An Expanded Benchmarking of Beyond-CMOS Devices Based on Boolean and Neuromorphic Representative Circuits. *IEEE Journal on Exploratory Solid-State Computational Devices and Circuits* **2017**, *3*, 101.
(5) Binek, C.; Doudin, B. Magnetoelectronics with magnetoelectrics. *J. Phys.: Condens. Matter* **2005**, *17*, L39.
(6) Bibes, M.; Barthélémy, A. Towards a magnetoelectric memory. *Nat. Mater.* **2008**, *7* (6), 425−426.
(7) Hu, J.-M.; Nan, C.-W. Opportunities and challenges for magnetoelectric devices. *APL Mater.* **2019**, *7* (8), 080905.
(8) Sharma, N.; Bird, J. P.; Binek, C.; Dowben, P. A.; Nikonov, D.; Marshall, A. Evolving magneto-electric device technologies. *Semicond. Sci. Technol.* **2020**, *35*, 073001.
(9) Fiebig, M.; Lottermoser, T.; Meier, D.; Trassin, M. The evolution of multiferroics. *Nat. Rev. Mater.* **2016**, *1* (8), 16046.
(10) Spaldin, N. A.; Ramesh, R. Advances in magnetoelectric multiferroics. *Nat. Mater.* **2019**, *18* (3), 203−212.
(11) Morgan, G. G.; Murnaghan, K. D.; Müller-Bunz, H.; McKee, V.; Harding, C. J. A Manganese(III) Complex That Exhibits Spin Crossover Triggered by Geometric Tuning. *Angew. Chem., Int. Ed.* **2006**, *45* (43), 7192−7195.
(12) Martinho, P. N.; Gildea, B.; Harris, M. M.; Lemma, T.; Naik, A. D.; Müller-Bunz, H.; Keyes, T. E.; Garcia, Y.; Morgan, G. G. Cooperative Spin Transition in a Mononuclear Manganese(III) Complex. *Angew. Chem., Int. Ed.* **2012**, *51* (50), 12597−12601.
(13) Halcrow, M. A. Spin-crossover Compounds with Wide Thermal Hysteresis. *Chem. Lett.* **2014**, *43* (8), 1178−1188.
(14) Pandurangan, K.; Gildea, B.; Murray, C.; Harding, C. J.; Müller-Bunz, H.; Morgan, G. G. Lattice Effects on the Spin-Crossover Profile of a Mononuclear Manganese(III) Cation. *Chem. - Eur. J.* **2012**, *18* (7), 2021−2029.
(15) Gildea, B.; Harris, M. M.; Gavin, L. C.; Murray, C. A.; Ortin, Y.; Müller-Bunz, H.; Harding, C. J.; Lan, Y.; Powell, A. K.; Morgan, G. G. Substituent Effects on Spin State in a Series of Mononuclear Manganese(III) Complexes with Hexadentate Schiff-Base Ligands. *Inorg. Chem.* **2014**, *53* (12), 6022−6033.
(16) Shatruk, M.; Phan, H.; Chrisostomo, B. A.; Suleimenova, A. Symmetry-breaking structural phase transitions in spin crossover complexes. *Coord. Chem. Rev.* **2015**, *289−290*, 62−73.
(17) Fitzpatrick, A. J.; Trzop, E.; Müller-Bunz, H.; Dîrtu, M. M.; Garcia, Y.; Collet, E.; Morgan, G. G. Electronic vs. structural ordering in a manganese(iii) spin crossover complex. *Chem. Commun.* **2015**, *51* (99), 17540−17543.
(18) Senthil Kumar, K.; Ruben, M. Emerging trends in spin crossover (SCO) based functional materials and devices. *Coord. Chem. Rev.* **2017**, *346*, 176−205.
(19) Brooker, S. Spin crossover with thermal hysteresis: practicalities and lessons learnt. *Chem. Soc. Rev.* **2015**, *44* (10), 2880−2892.
(20) Mason, H. E.; Li, W.; Carpenter, M. A.; Hamilton, M. L.; Howard, J. A. K.; Sparkes, H. A. Structural and spectroscopic characterisation of the spin crossover in [Fe(abpt)2(NCS)2] polymorph A. *New J. Chem.* **2016**, *40* (3), 2466−2478.
(21) Ortega-Villar, N.; Muñoz, M. C.; Real, J. A. Symmetry Breaking in Iron(II) Spin-Crossover Molecular Crystals. *Magnetochemistry* **2016**, *2* (1), 16.
(22) Collet, E.; Guionneau, P. Structural analysis of spin-crossover materials: From molecules to materials. *C. R. Chim.* **2018**, *21* (12), 1133−1151.
(23) Otsuki, Y.; Kimura, S.; Awaji, S.; Nakano, M. Magneto-capacitance effect and magnetostriction by the field-induced spin-crossover in [MnIII(taa)]. *AIP Adv.* **2019**, *9* (8), 085219.
(24) Nakano, M.; Matsubayashi, G.-e.; Matsuo, T. Dielectric behavior of manganese(III) spin-crossover complex [Mn(taa)]. *Phys. Rev. B: Condens. Matter Mater. Phys.* **2002**, *66* (21), 212412.
(25) Chikara, S.; Gu, J.; Zhang, X. G.; Cheng, H.-P.; Smythe, N.; Singleton, J.; Scott, B.; Krenkel, E.; Eckert, J.; Zapf, V. S. Magnetoelectric behavior via a spin state transition. *Nat. Commun.* **2019**, *10* (1), 4043.
(26) Lefter, C.; Tan, R.; Dugay, J.; Tricard, S.; Molnár, G.; Salmon, L.; Carrey, J.; Nicolazzi, W.; Rotaru, A.; Bousseksou, A. Unidirectional electric field-induced spin-state switching in spin crossover based microelectronic devices. *Chem. Phys. Lett.* **2016**, *644*, 138−141.
(27) Zhang, X.; Palamarciuc, T.; Létard, J.-F.; Rosa, P.; Lozada, E. V.; Torres, F.; Rosa, L. G.; Doudin, B.; Dowben, P. A. The spin state of a molecular adsorbate driven by the ferroelectric substrate polarization. *Chem. Commun.* **2014**, *50* (18), 2255−2257.
(28) Jornet-Mollá, V.; Duan, Y.; Giménez-Saiz, C.; Tang, Y.-Y.; Li, P.-F.; Romero, F. M.; Xiong, R.-G. A Ferroelectric Iron(II) Spin Crossover Material. *Angew. Chem., Int. Ed.* **2017**, *56* (45), 14052−14056.
(29) Qi, Y.; Müller, E. W.; Spiering, H.; Gütlich, P. The effect of a magnetic field on the high-spin α low-spin transition in [Fe(phen)-2(NCS)2]. *Chem. Phys. Lett.* **1983**, *101* (4), 503−505.
(30) Lejay, J.; Jansen, A. G. M.; Wyder, P.; Bronger, W.; Kläui, W. Spin equilibrium of Co3+ complexes influenced by a magnetic field. *Phys. Rev. B: Condens. Matter Mater. Phys.* **1991**, *43* (10), 8196−8198.
(31) Garcia, Y.; Kahn, O.; Ader, J.-P.; Buzdin, A.; Meurdesoif, Y.; Guillot, M. The effect of a magnetic field on the inversion temperature of a spin crossover compound revisited. *Phys. Lett. A* **2000**, *271* (1), 145−154.
(32) Negre, N.; Goiran, M.; Bousseksou, A.; Haasnoot, J.; Boukheddaden, K.; Askenazy, S.; Varret, F. High magnetic field induced spin transition, H.M.F.I.S.T. effect, in [Fe0.52Ni0.48(btr)2-(NCS)2]H_2O. *Synth. Met.* **2000**, *115* (1), 289−292.
(33) Bousseksou, A.; Negre, N.; Goiran, M.; Salmon, L.; Tuchagues, J.-P.; Boillot, M.-L.; Boukheddaden, K.; Varret, F. Dynamic triggering of a spin-transition by a pulsed magnetic field. *Eur. Phys. J. B* **2000**, *13* (3), 451−456.
(34) Kimura, S.; Narumi, Y.; Kindo, K.; Nakano, M.; Matsubayashi, G.-e. Field-induced spin-crossover transition of [MnIII(taa)] studied under pulsed magnetic fields. *Phys. Rev. B: Condens. Matter Mater. Phys.* **2005**, *72* (6), 064448.

https://dx.doi.org/10.1021/acs.inorgchem.0c02789
Inorg. Chem. XXXX, XXX, XXX−XXX

(35) Altarawneh, M. M.; Chern, G. W.; Harrison, N.; Batista, C. D.; Uchida, A.; Jaime, M.; Rickel, D. G.; Crooker, S. A.; Mielke, C. H.; Betts, J. B.; Mitchell, J. F.; Hoch, M. J. R. Cascade of Magnetic Field Induced Spin Transitions in LaCoO3. *Phys. Rev. Lett.* **2012**, *109* (3), 037201.
(36) Ridier, K.; Bas, A.-C.; Zhang, Y.; Routaboul, L.; Salmon, L.; Molnár, G.; Bergaud, C.; Bousseksou, A. Unprecedented switching endurance affords for high-resolution surface temperature mapping using a spin-crossover film. *Nat. Commun.* **2020**, *11*, 3611.
(37) Ridier, K.; Bas, A. C.; Shalabaeva, V.; Nicolazzi, W.; Salmon, L.; Molnár, G.; Bousseksou, A.; Lorenc, M.; Bertoni, R.; Collet, E.; Cailleau, H. Finite Size Effects on the Switching Dynamics of Spin-Crossover Thin Films Photoexcited by a Femtosecond Laser Pulse. *Adv. Mater.* **2019**, *31*, 1901361.
(38) Piedrahita-Bello, M.; Martin, B.; Salmon, L.; Molnár, G.; Demont, P.; Bousseksou, A. Mechano-electric coupling in P(VDF−TrFE)/spin crossover composites†. *J. Mater. Chem. C* **2020**, *8*, 6042.
(39) Mosey, A.; Dale, A. S.; Hao, G.; N'Diaye, A.; Dowben, P. A.; Cheng, R. Quantitative Study of the Energy Changes in Voltage-Controlled Spin Crossover Molecular Thin Films. *J. Phys. Chem. Lett.* **2020**, *11*, 8231.
(40) Weber, B.; Dowben, P. Preface to the JPCM Special Issue on Molecular Magnetism. *J. Phys.: Condens. Matter* **2020**, *32*, 440201.
(41) Jakobsen, V. B.; Trzop, E.; Gavin, L. C.; Dobbelaar, E.; Chikara, S.; Ding, X.; Esien, K.; Müller-Bunz, H.; Felton, S.; Zapf, V. S.; Collet, E.; Carpenter, M. A.; Morgan, G. G. Stress-Induced Domain Wall Motion in a Ferroelastic Mn3+ Spin Crossover Complex. *Angew. Chem., Int. Ed.* **2020**, *59* (32), 13305−13312.
(42) Molnár, G.; Rat, S.; Salmon, L.; Nicolazzi, W.; Bousseksou, A. Spin Crossover Nanomaterials: From Fundamental Concepts to Devices. *Adv. Mater.* **2018**, *30* (5), 1703862.
(43) Létard, J.-F. Photomagnetism of iron(ii) spin crossover complexes—the T(LIESST) approach. *J. Mater. Chem.* **2006**, *16* (26), 2550−2559.
(44) Sato, O. Dynamic molecular crystals with switchable physical properties. *Nat. Chem.* **2016**, *8* (7), 644−656.
(45) Chastanet, G.; Lorenc, M.; Bertoni, R.; Desplanches, C. Light-induced spin crossover—Solution and solid-state processes. *C. R. Chim.* **2018**, *21* (12), 1075−1094.
(46) Zapf, V. S.; Sengupta, P.; Batista, C. D.; Nasreen, F.; Wolff-Fabris, F.; Paduan-Filho, A. Magnetoelectric effects in an organo-metallic quantum magnet. *Phys. Rev. B: Condens. Matter Mater. Phys.* **2011**, *83* (14), 140405.
(47) Pardo, E.; Train, C.; Liu, H.; Chamoreau, L.-M.; Dkhil, B.; Boubekeur, K.; Lloret, F.; Nakatani, K.; Tokoro, H.; Ohkoshi, S.-i.; Verdaguer, M. Multiferroics by Rational Design: Implementing Ferroelectricity in Molecule-Based Magnets. *Angew. Chem., Int. Ed.* **2012**, *51* (33), 8356−8360.
(48) Tian, Y.; Stroppa, A.; Chai, Y.; Yan, L.; Wang, S.; Barone, P.; Picozzi, S.; Sun, Y. Cross coupling between electric and magnetic orders in a multiferroic metal-organic framework. *Sci. Rep.* **2015**, *4*, 6062.
(49) Mun, E.; Weickert, F.; Kim, J.; Scott, B. L.; Miclea, C. F.; Movshovich, R.; Wilcox, J.; Manson, J.; Zapf, V. S. Partially disordered antiferromagnetism and multiferroic behavior in a frustrated Ising system CoCl2−2SC(NH2)2. *Phys. Rev. B: Condens. Matter Mater. Phys.* **2016**, *93* (10), 104407.
(50) Gómez-Aguirre, L. C.; Pato-Doldán, B.; Mira, J.; Castro-García, S.; Señarís-Rodríguez, M. A.; Sánchez-Andújar, M.; Singleton, J.; Zapf, V. S. Magnetic Ordering-Induced Multiferroic Behavior in [CH3NH3][Co(HCOO)3] Metal−Organic Framework. *J. Am. Chem. Soc.* **2016**, *138* (4), 1122−1125.
(51) Jain, P.; Stroppa, A.; Nabok, D.; Marino, A.; Rubano, A.; Paparo, D.; Matsubara, M.; Nakotte, H.; Fiebig, M.; Picozzi, S.; Choi, E. S.; Cheetham, A. K.; Draxl, C.; Dalal, N. S.; Zapf, V. S. Switchable electric polarization and ferroelectric domains in a metal-organic-framework. *npj Quantum Mater.* **2016**, *1*, 16012.
(52) Aoyama, T.; Yamauchi, K.; Iyama, A.; Picozzi, S.; Shimizu, K.; Kimura, T. Giant spin-driven ferroelectric polarization in TbMnO3 under high pressure. *Nat. Commun.* **2014**, *5* (1), 4927.
(53) Miyashita, S.; Konishi, Y.; Tokoro, H.; Nishino, M.; Boukheddaden, K.; Varret, F. Structures of Metastable States in Phase Transitions with a High-Spin Low-Spin Degree of Freedom. *Prog. Theor. Phys.* **2005**, *114* (4), 719−735.
(54) Varret, F.; Slimani, A.; Boukheddaden, K.; Chong, C.; Mishra, H.; Collet, E.; Haasnoot, J.; Pillet, S. The propagation of the thermal spin transition of [Fe(btr)2(NCS)2]·H_2O single crystals, observed by optical microscopy. *New J. Chem.* **2011**, *35* (10), 2333−2340.
(55) Slimani, A.; Varret, F.; Boukheddaden, K.; Garrot, D.; Oubouchou, H.; Kaizaki, S. Velocity of the High-Spin Low-Spin Interface Inside the Thermal Hysteresis Loop of a Spin-Crossover Crystal, via Photothermal Control of the Interface Motion. *Phys. Rev. Lett.* **2013**, *110* (8), 087208.
(56) Sy, M.; Varret, F.; Boukheddaden, K.; Bouchez, G.; Marrot, J.; Kawata, S.; Kaizaki, S. Structure-Driven Orientation of the High-Spin−Low-Spin Interface in a Spin-Crossover Single Crystal. *Angew. Chem.* **2014**, *126* (29), 7669−7672.
(57) Paez-Espejo, M.; Sy, M.; Boukheddaden, K. Elastic Frustration Causing Two-Step and Multistep Transitions in Spin-Crossover Solids: Emergence of Complex Antiferroelastic Structures. *J. Am. Chem. Soc.* **2016**, *138* (9), 3202−3210.
(58) Traiche, R.; Sy, M.; Oubouchou, H.; Bouchez, G.; Varret, F.; Boukheddaden, K. Spatiotemporal Observation and Modeling of Remarkable Temperature Scan Rate Effects on the Thermal Hysteresis in a Spin-Crossover Single Crystal. *J. Phys. Chem. C* **2017**, *121* (21), 11700−11708.
(59) Fourati, H.; Milin, E.; Slimani, A.; Chastanet, G.; Abid, Y.; Triki, S.; Boukheddaden, K. Interplay between a crystal's shape and spatiotemporal dynamics in a spin transition material. *Phys. Chem. Chem. Phys.* **2018**, *20* (15), 10142−10154.
(60) Affes, K.; Fourati, H.; Slimani, A.; Boukheddaden, K. Effects of High-Spin-Low-Spin Lattice Misfit on the Nucleation and Propagation Velocities of Elastic Interfaces in Cooperative Spin-Crossover Solids. *J. Phys. Soc. Jpn.* **2019**, *88* (12), 124701.
(61) Chernyshov, D.; Bürgi, H.-B.; Hostettler, M.; Törnroos, K. W. Landau theory for spin transition and ordering phenomena in Fe(II) compounds. *Phys. Rev. B: Condens. Matter Mater. Phys.* **2004**, *70* (9), 094116.
(62) Watanabe, H.; Tanaka, K.; Bréfuel, N.; Cailleau, H.; Létard, J.-F.; Ravy, S.; Fertey, P.; Nishino, M.; Miyashita, S.; Collet, E. Ordering phenomena of high-spin/low-spin states in stepwise spin-crossover materials described by the ANNNI model. *Phys. Rev. B: Condens. Matter Mater. Phys.* **2016**, *93* (1), 014419.
(63) Jia, C.-L.; Mi, S.-B.; Urban, K.; Vrejoiu, I.; Alexe, M.; Hesse, D. Atomic-scale study of electric dipoles near charged and uncharged domain walls in ferroelectric films. *Nat. Mater.* **2008**, *7* (1), 57−61.
(64) Li, L.; Gao, P.; Nelson, C. T.; Jokisaari, J. R.; Zhang, Y.; Kim, S.-J.; Melville, A.; Adamo, C.; Schlom, D. G.; Pan, X. Atomic Scale Structure Changes Induced by Charged Domain Walls in Ferroelectric Materials. *Nano Lett.* **2013**, *13* (11), 5218−5223.
(65) Bednyakov, P. S.; Sturman, B. I.; Sluka, T.; Tagantsev, A. K.; Yudin, P. V. Physics and applications of charged domain walls. *npj Comput. Mater.* **2018**, *4* (1), 65.
(66) Ohtomo, A.; Hwang, H. Y. A high-mobility electron gas at the LaAlO3/SrTiO3 heterointerface. *Nature* **2004**, *427* (6973), 423−426.
(67) Nakagawa, N.; Hwang, H. Y.; Muller, D. A. Why some interfaces cannot be sharp. *Nat. Mater.* **2006**, *5* (3), 204−209.
(68) Galperin, M.; Ratner, M. A.; Nitzan, A. Hysteresis, Switching, and Negative Differential Resistance in Molecular Junctions: A Polaron Model. *Nano Lett.* **2005**, *5* (1), 125−130.
(69) Punk, M.; Dumitrescu, P. T.; Zwerger, W. Polaron-to-molecule transition in a strongly imbalanced Fermi gas. *Phys. Rev. A: At., Mol., Opt. Phys.* **2009**, *80* (5), 053605.
(70) Rotaru, A.; Gural'skiy, I. y. A.; Molnár, G.; Salmon, L.; Demont, P.; Bousseksou, A. Spin state dependence of electrical conductivity of spin crossover materials. *Chem. Commun.* **2012**, *48* (35), 4163−4165.

https://dx.doi.org/10.1021/acs.inorgchem.0c02789
Inorg. Chem. XXXX, XXX, XXX−XXX

(71) Lefter, C.; Davesne, V.; Salmon, L.; Molnár, G.; Demont, P.; Rotaru, A.; Bousseksou, A. Charge Transport and Electrical Properties of Spin Crossover Materials: Towards Nanoelectronic and Spintronic Devices. *Magnetochemistry* **2016**, *2* (1), 18.

https://dx.doi.org/10.1021/acs.inorgchem.0c02789
Inorg. Chem. XXXX, XXX, XXX−XXX